RESEARCH ARTICLE | MARCH 24 2010

Kinetics of the mildly relativistic plasma and GRBs

A. G. Aksenov; R. Ruffini; G. V. Vereshchagin

AIP Conf. Proc. 1205, 11–16 (2010)
https://doi.org/10.1063/1.3382316

Kinetics of the mildly relativistic plasma and GRBs

A.G. Aksenov*, R. Ruffini† and G.V. Vereshchagin†

*Institute for Computer-Aided Design, Russian Academy of Sciences, Vtoraya Brestskaya 19/18, 123056 Moscow, Russia

†ICRANet p.le della Republica, 10, 65100 Pescara, Italy and ICRA and University of Rome "Sapienza", Physics Department, p.le A. Moro 5, 00185 Rome, Italy

Abstract. We consider optically thick photon-pair-proton plasma in the framework of Boltzmann equations. For the sake of simplicity we consider the uniform and isotropic plasma. It has been shown that arbitrary initial distribution functions evolve to the thermal equilibrium state through so called kinetic equilibrium state with common temperature of all particles and nonzero chemical potentials. For the plasma temperature 0.1–10 MeV relevant for GRB (Gamma-Ray Burst) sources we evaluate the thermalization time scale as function of total energy density and baryonic loading parameter.

INTRODUCTION

Pair plasma has been considered in the literature in connection with its possible existence in astrophysical sources [1]-[6]. In particular, its role in GRBs has been realized quite early [7]-[9], and for its description hydrodynamic treatment has been usually adopted. In many compact astrophysical sources the characteristic time scales (e.g. radiation loss, hydrodynamic expansion) may be short enough, and plasma created by some nonequilibrium process may not have time to relax to thermal equilibrium. Consequently, hydrodynamic approximation usually adopted for simplicity may not necessary be valid. Thus it is crucial to know relaxation time scales for relativistic pair plasma. In what follows we will consider for definiteness pair plasma in GRB sources, exploring wide range of plasma energy densities.

Based on isotropic energy release in GRB sources

$$10^{48} \leq E_0 \leq 10^{54}\text{ergs}, \tag{1}$$

and time variability of the prompt emission, converted into the source size [8]

$$10^6 \leq R_0 \leq 10^8 \text{ cm}. \tag{2}$$

one can estimate the total energy density in such sources

$$10^{23} \leq \rho \leq 10^{35} \text{ erg/cm}^3, \tag{3}$$

and then convert it into temperature, assuming the plasma is in thermal equilibrium

$$0.1 \leq k_B T_{\rm th} \leq 100 \text{ MeV}, \tag{4}$$

where k_B is Boltzmann's constant. For such temperatures plasma can generate electron-positron pairs or photons, even if initially it contains only one kind of these particles: either pairs or photons. However such temperatures are not sufficiently high to generate heavy particles such as muon-antimuon or proton-antiproton pairs. Therefore one can assume the number of protons to be constant.

The plasma can be either transparent or optically thick to neutrinos. The energy loss due to neutrino can be estimated as [10]

$$\frac{1}{\rho_\gamma}\frac{d\rho}{dt}\Delta t \simeq 3.6\cdot 10^{-3}\left(\frac{k_B T}{m_e c^2}\right)^5 \frac{\Delta t}{1\,\text{sec}}, \tag{5}$$

where m_e is the electron mass, and $k_{\rm B}$ is Boltzmann's constant, c is the speed of light. For GRBs with the dynamical time $\Delta t \sim 10^{-3}$ sec, the energy loss due to neutrinos becomes relevant for high temperatures $k_B T > 5$ MeV [11]. However, on the time scale of relaxation to thermal equilibrium $\Delta t \leq 10^{-11}$ sec the energy loss is negligible.

Another important property of considered plasma is small plasma parameter $g = (n\lambda_D)^3 \ll 1$, there λ_D is the Debye length. Given its smallness one can use one-particle distribution functions for particles of i-kind $f(\mathbf{r},\mathbf{p},t)$.

In addition, electrons and positrons can be treated as nondegenerate at such temperatures (degeneracy becomes essential near the upper limit of the temperature). This property however simplifies calculations.

Attempts to determine relaxation time scales of optically thick electron-positron plasmas has been started in 1980s, see e.g. [4, 5]. However, they were computed using various approximations such as ultrarelativistic electrons as in [4], or constant Coulomb logarithm as in [5]. The major difficulty in such computations comes from the nonlinearity of the reaction rates as functions of particles energy, and also from the interference of different microphysical processes. Therefore, to determine such time scales one has to solve numerically the relativis-

CP1205, *The Sun, The Stars, The Universe and General Relativity*
edited by R. Ruffini and G. Vereshchagin

Table 1. Microphysical processes in the pair plasma.

Binary interactions	Radiative variants
Møller, Bhabha $e^{\pm}e^{\pm\prime} \leftrightarrow e^{\pm\prime\prime}e^{\pm\prime\prime\prime}$ $e^{\pm}e^{\mp} \leftrightarrow e^{\pm\prime}e^{\mp\prime}$	Bremsstrahlung $e^{\pm}e^{\pm\prime}\leftrightarrow e^{\pm\prime\prime}e^{\pm\prime\prime\prime}\gamma$ $e^{\pm}e^{\mp}\leftrightarrow e^{\pm\prime}e^{\mp\prime}\gamma$
Single Compton $e^{\pm}\gamma\leftrightarrow e^{\pm}\gamma'$	Double Compton $e^{\pm}\gamma\leftrightarrow e^{\pm\prime}\gamma'\gamma''$
Pair production and annihilation $\gamma\gamma'\leftrightarrow e^{\pm}e^{\mp}$	Radiative pair production and three photon annihilation $\gamma\gamma'\leftrightarrow e^{\pm}e^{\mp}\gamma''$ $e^{\pm}\gamma\leftrightarrow e^{\pm\prime}e^{\mp}e^{\pm\prime\prime}$ $e^{\pm}e^{\mp}\leftrightarrow\gamma\gamma'\gamma''$

Table 2. Microphysical processes with protons.

Binary interactions	Radiative and pair production variants
Coulomb scattering $p_1p_2 \longrightarrow p_1'p_2'$ $pe^{\pm} \longrightarrow p'e^{\pm\prime}$	Bremsstrahlung $p_1p_2 \leftrightarrow p_1'p_2'\gamma$ $pe^{\pm} \leftrightarrow p'e^{\pm\prime}\gamma$ $pe_1^{\pm} \leftrightarrow p'e_1^{\pm\prime}e^{\pm}e^{\mp}$
Single Compton $p\gamma \longrightarrow p'\gamma'$	Double Compton $p\gamma \leftrightarrow p'\gamma'\gamma''$ $p\gamma \leftrightarrow p'e^{\pm}e^{\mp}$

tic Boltzmann equation with all the corresponding collisional integrals.

We consider homogeneous and isotropic optically thick plasma and follow its kinetic evolution toward thermal equilibrium. For the relevance of three-particle interactions in the pure pair plasma see [12]. Details about the computational scheme as well as extension to the proton admixture case are given in [13]. Our goal here is to compute the corresponding time scales for a range of the following two parameters: the total energy density and the baryonic loading. We provide the scheme for the computation of relevant time scales.

BOLTZMANN EQUATIONS

We solve numerically the relativistic Boltzmann equations [14], [15] for photons, electrons, positrons, and protons

$$\frac{1}{c}\frac{\partial f_i}{\partial t} = \sum_q (\eta_i^q - \chi_i^q f_i), \tag{6}$$

where $f_i(\varepsilon,t)$ are their distribution functions, the index i denotes the type of the particle, ε is it's energy, and η_i^q, χ_i^q are the emission and the absorption coefficients for the production of i-particle via the reaction labeled by q. We consider all possible binary and triple interactions between electrons, positrons, photons, and protons as summarized in Table 1, and Table 2.

In the case of pure (neutral) pair plasma electron and proton distribution functions are equal, $f_- = f_+$. When protons are present one should solve Boltzmann equations (6) for four distribution functions f_γ, f_-, f_+, f_p.

We explore the parameter space given by the total energy density ρ (which includes rest mass of protons), and the baryonic loading

$$B \equiv \frac{\rho_p}{\rho_\gamma + \rho_\pm}, \tag{7}$$

confined as

$$10^{-3} \le B \le 10^{3}. \tag{8}$$

This range of the baryonic loading allows to explore different regimes: the case of radiation-dominated plasma composed essentially by electron-positron pairs and photons for low values of B, and the case of matter-dominated electron-proton plasma for the upper values of B.

In the previous works [12, 13] we used arbitrary nonequlibrium initial states and showed that independent on the functional form of initial distribution functions the plasma evolves to thermal equilibrium state. Therefore we select initial spectra of particles given by the distribution functions

$$f_i(\varepsilon) = \exp\left(-\frac{\varepsilon - \varphi_i}{\theta_i}\right), \tag{9}$$

where $\varepsilon_i = \varepsilon/(m_ic^2)$ is the energy of the particles, $\varphi_i \equiv \mu_i/(m_ic^2)$ and $\theta_i \equiv k_{\rm B}T_i/(m_ic^2)$ are their chemical potentials and temperatures.

In such case the above mentioned two parameters define completely the characteristic time of the evolution of the plasma to the thermal equilibrium. Since it is easy to write down the expressions for total energy density through the proton number density n_p and temperature θ we will use the auxiliary quantity

$$B' \equiv \frac{\rho_p}{\rho} = \frac{1}{1+B^{-1}} \approx \frac{m_pc^2n_p}{\rho}, \tag{10}$$

where m_p is the proton mass.

Without loss of generality we take $\varphi_- = -\varphi_+ = \varphi_e$, $\varphi_\gamma = 0$ and $\theta_- = \theta_+ = \theta_e$. Then one can calculate the φ_e/θ_e from the electroneutrality condition (details in [13])

$$2\sinh\left(\frac{\varphi_e}{\theta_e}\right) = n_pV_0,\ V_0 = \pi^2\left(\frac{\hbar}{m_ec}\right)^3, \tag{11}$$

and the total energy density is

$$\rho = \frac{m_e c^2}{V_0}\left\{6\theta_\gamma^4 + \left[(n_p V_0)^2 + 4\theta_e^2 K_2(\theta_e^{-1})^2\right]^{\frac{1}{2}} \times \right.$$
$$\left. \times \frac{3K_3(\theta_e^{-1})+K_1(\theta_e^{-1})}{4K_2(\theta_e^{-1})}\right\} + n_p m_p c^2\left(1+\tfrac{3}{2}\tfrac{m_e}{m_p}\theta_p\right). \quad (12)$$

For the computations in all the parameter space (ρ, B') we take the coefficients c_γ, c_e, c_p for $\theta_\gamma = c_\gamma\theta$, $\theta_e = c_e\theta$, $\theta_p = c_p\theta$ with hot photons $c_\gamma = 2$, cold pairs $c_e = 1/2$, and cold protons $c_p = 1/4$. The parameter θ then satisfies the energy density formula (12).

NUMERICAL SCHEME

Our goal is to construct the conservative scheme which implements baryon number, charge and energy conservation. For this reason we prefer to use, instead of distribution functions f_i, spectral energy densities

$$E_i(\varepsilon_i) = \frac{4\pi\varepsilon_i^3\beta_i f_i}{c^3}, \quad (13)$$

where $\beta_i = \sqrt{1-(m_i c^2/\varepsilon_i)^2}$, in the phase space ε_i. Then

$$\varepsilon_i f_i(\mathbf{p},t)d\mathbf{r}d\mathbf{p} = \frac{4\pi\varepsilon^3\beta_i f_i}{c^3}\mathbf{r}d\varepsilon_i = E_i d\mathbf{r}d\varepsilon_i \quad (14)$$

is the energy in the volume of the phase space $d\mathbf{r}d\mathbf{p}$. The particle density is

$$n_i = \int f_i d\mathbf{p} = \int \frac{E_i}{\varepsilon_i}d\varepsilon_i,\ dn_i = f_i d\mathbf{p}. \quad (15)$$

We can rewrite Boltzmann equations (6) in the form

$$\frac{1}{c}\frac{\partial E_i}{\partial t} = \sum_q(\tilde{\eta}_i^q - \chi_i^q E_i), \quad (16)$$

where $\eta_i^q = (4\pi\varepsilon_i^3\beta_i/c^3)\tilde{\eta}_i^q$.

We introduced the computational grid in the phase space $\{\varepsilon_i, \mu, \varphi\}$, where $\mu = \cos\theta$, θ and φ are angles between radius vector $\mathbf{r}$ and the particle momentum $\mathbf{p}$. The zone boundaries are $\varepsilon_{i,\omega\mp1/2}$, $\mu_{k\mp1/2}$, $\varphi_{l\mp1/2}$ for $1 \le \omega \le \omega_{\max}$, $1 \le k \le k_{\max}$, $1 \le l \le l_{\max}$. The length of the i-th interval is $\Delta\varepsilon_{i,\omega} \equiv \varepsilon_{i,\omega+1/2} - \varepsilon_{i,\omega-1/2}$. On the finite grid the functions (13) become

$$E_{i,\omega} \equiv \frac{1}{\Delta\varepsilon_{i,\omega}}\int_{\Delta\varepsilon_{i,\omega}} d\varepsilon E_i(\varepsilon). \quad (17)$$

Now one can replace the collisional integrals in (16) by the corresponding sums. After this procedure we get the set of ordinary differential equations (ODE's), instead of the system of partial differential equations for the quantities $E_{i,\omega}$ to be solved.

There are several characteristic times for different processes in the problem, and therefore our system of differential equations is stiff. It means eigenvalues of Jacobi matrix differs significantly, and the real parts of eigenvalues are negative. We use Gear's method [16] to integrate ODE's numerically. This implicit method has been developed for stiff ODE's. Besides, the method we use is conservative for the number of particles, where appropriate.

To get more details of the method consider for instance the Compton scattering. Neglecting degeneracy effects which are usually accounted for as induced radiation and occupied states the emission and absorption coefficients for photons are [17], [18]

$$\tilde{\eta}_\gamma^{\mathrm{Cs}}(\mathbf{k}) = \int d\mathbf{k}' d\mathbf{p} d\mathbf{p}' V w_{\mathbf{k}',\mathbf{p}';\mathbf{k},\mathbf{p}} f_\gamma(\mathbf{k}') f_e(\mathbf{p}',t), \quad (18)$$

$$\chi_\gamma^{\mathrm{Cs}} f_\gamma(\mathbf{k}) = \int d\mathbf{k}' d\mathbf{p} d\mathbf{p}' V w_{\mathbf{k}',\mathbf{p}';\mathbf{k},\mathbf{p}} f_\gamma(\mathbf{k}) f_e(\mathbf{p},t), \quad (19)$$

where $w_{\mathbf{k}',\mathbf{p}';\mathbf{k},\mathbf{p}} = \frac{\hbar^2 c^6}{(2\pi)^2 V}\delta(\varepsilon_\gamma + \varepsilon_e - \varepsilon_\gamma' - \varepsilon_e')\delta(\mathbf{k}+\mathbf{p}-\mathbf{k}'-\mathbf{p}')\frac{|M_{fi}|^2}{16\varepsilon_\gamma\varepsilon_e\varepsilon_\gamma'\varepsilon_e'}$ is the probability of the process, the matrix element $M_{fi}(s,u)$ [19] depends on the kinematic invariants $s = (\mathfrak{p}+\mathfrak{k})^2$ and $u = (\mathfrak{p}-\mathfrak{k}')^2$, $\mathfrak{k} = (\varepsilon_\gamma/c)(1,\mathbf{e}_\gamma)$ and $\mathfrak{p} = (\varepsilon_e/c)(1,\beta\mathbf{e}_e)$ are four energy-momentum vectors of photons and electrons, respectively, and $d\mathbf{p} = d\varepsilon do\varepsilon^2\beta/c^3$, and $do = d\mu d\phi$, $\mathbf{p}$ is the momentum of electrons, while $\mathbf{k}$ is the momentum of photons.

In order to calculate e.g. the absorption coefficient $\chi_\gamma^{\mathrm{Cs}}$ we proceed as follows. Substituting the expression for the probability w from equation (18) we can make one integration over $d\mathbf{p}'$

$$\int d\mathbf{p}'\delta(d\mathbf{k}+d\mathbf{p}-d\mathbf{k}'-d\mathbf{p}') \to 1, \quad (20)$$

but we should take into account fixed relation

$$\mathbf{p}' = \mathbf{k}+\mathbf{p}-\mathbf{k}'. \quad (21)$$

In the next integration over $d\mathbf{k}' = d\varepsilon_\gamma'\varepsilon_\gamma'^2 d\omega_\gamma'/c^3$ we have $\int d\varepsilon_\gamma'\delta(\varepsilon_\gamma+\varepsilon_e-\varepsilon_\gamma'-\varepsilon_e') = \int d(\varepsilon_\gamma'+\varepsilon_e')\frac{1}{|\partial(\varepsilon_\gamma'+\varepsilon_e')/\partial\varepsilon_\gamma'|}\delta(\varepsilon_\gamma+\varepsilon_e-\varepsilon_\gamma'-\varepsilon_e') \to \frac{1}{|\partial(\varepsilon_\gamma'+\varepsilon_e')/\partial\varepsilon_\gamma'|} \equiv J_1$. Finally, we have

$$\chi_\gamma^{\mathrm{Cs}} = \int do_\gamma' d\mathbf{p} J_1 \frac{c\varepsilon_\gamma'|M_{fi}|^2\hbar^2c^2}{16\varepsilon_e\varepsilon_\gamma\varepsilon_e'} f_e(\mathbf{p},t), \quad (22)$$

where

$$\varepsilon_\gamma' = \frac{\varepsilon_e\varepsilon_\gamma(1-\beta\mathbf{b}_e\mathbf{b}_\gamma)}{\varepsilon_e(1-\beta\mathbf{b}_e\mathbf{b}_\gamma') + \varepsilon_\gamma(1-\mathbf{b}_\gamma\mathbf{b}_\gamma')}, \quad (23)$$

$\varepsilon_e' = \varepsilon_e + \varepsilon_\gamma - \varepsilon_\gamma'$, $\mathbf{b}_i = \mathbf{p}_i/p$, $\mathbf{b}_i' = \mathbf{p}_i'/p'$, $\mathbf{b}_e' = (\beta\varepsilon_e\mathbf{b}_e + \varepsilon_\gamma\mathbf{b}_\gamma - \varepsilon_\gamma'\mathbf{b}_\gamma')/(\beta'\varepsilon_e')$.

The average absorption coefficient on the finite grid is $(\chi E)^{\rm Cs}_{\gamma,\omega} \equiv \frac{\int_{\varepsilon_\gamma\in\Delta\varepsilon_{\gamma,\omega}} d\varepsilon_\gamma \chi^{\rm Cs}_\gamma E_\gamma}{\Delta\varepsilon_{\gamma,\omega}} = \frac{1}{\Delta\varepsilon_{\gamma,\omega}} \int_{\varepsilon_\gamma\in\Delta\varepsilon_{\gamma,\omega}} dn_\gamma dn_e do'_\gamma J_1 \frac{\varepsilon'_\gamma |M_{fi}|^2 \bar{h}^2 c^2}{16\varepsilon_e\varepsilon'_e}$.

Similar integrations can be performed for the emission term, and we have $\eta^{\rm Cs}_{\gamma,\omega,k} \equiv \frac{\int_{\varepsilon'_\gamma\in\Delta\varepsilon_{\gamma,\omega}} d\varepsilon_\gamma d\mu_\gamma \eta^{\gamma e\to\gamma' e'}_\gamma \mu'_{\gamma\in\Delta\mu_k}}{\Delta\varepsilon_{\gamma,\omega}\Delta\mu_k} = \frac{1}{\Delta\varepsilon_{\gamma,\omega}\Delta\mu_k} \int_{\substack{\varepsilon'_\gamma\in\Delta\varepsilon_{\gamma,\omega} \\ \mu'_\gamma\in\Delta\mu_k}} dn_\gamma dn_e do'_\gamma J_1 \frac{\varepsilon'^2_\gamma |M_{fi}|^2 \bar{h}^2 c^2}{16\varepsilon_e\varepsilon_\gamma\varepsilon'_e}$. Both the exact energy conservation law and the particles number conservation law are satisfied as we adopt interpolation of grig functions $E_{i\omega}$ inside the energy intervals.

Details of calculation of all reactions can be found in [13].

DETERMINATION OF THE THERMALIZATION TIME SCALE

Each of the above reactions is characterized by the corresponding time scale τ and optical depth $\tau^\star$. For Compton scattering, for instance, we have

$$\tau_{\rm cs} = \frac{1}{\sigma_{\rm T} n_\pm c},\ \tau^\star_{\rm cs} = \sigma_{\rm T} n_\pm R_0, \qquad (24)$$

where $\sigma_{\rm T}$ is the Thomson cross section, R_0 is the size of plasma, and $n_\pm$ is the number density of pairs. For pairs and photons there are two time scales in our problem that characterize the condition of detailed balance between direct and inverse reactions, $\tau_{2p} \simeq t_{\rm cs}$ for binary and $\tau_{3p} \simeq \alpha^{-1} t_{\rm cs}$ for triple interactions, respectively.

In order to illustrate the concept of detailed balance consider the properties of the distribution functions (9) with different temperatures θ_i and chemical potentials ϕ_i for pairs and photons. The requirement of vanishing reaction rate for the Compton scattering $f_\pm f_\gamma = f'_\pm f'_\gamma$ leads to the equal temperature of pairs and photons $\theta_\pm = \theta_\gamma \equiv \theta_k$; see also [12, 13]. In this way the detailed balance between any direct and the corresponding inverse reactions shown in Table 1 leads to relations between θ and ϕ collected in Table 3.

In the first phase of the system evolution the binary interactions are faster. Starting from arbitrary distribution functions we find a common development: at the time $t_{\rm cs}$ the distribution functions always have evolved in a functional form on the entire energy range, depending only on two parameters. We find in fact for the distribution functions the expressions (9), see [13]. Such a configuration corresponds to a kinetic equilibrium [20] in which electrons, positrons, and photons acquire a common temperature and nonzero chemical potential. At the same time we found that triple interactions become essential for $t > t_{\rm cs}$,

Table 3. Relations between parameters of equilibrium distribution functions fulfilling detailed balance conditions for each of the reactions shown in Table 1.

Interaction	Parameters of distribution functions
Compton scattering	$\theta_\gamma = \theta_\pm$, $\forall\phi_\gamma, \phi_\pm$
Pair production	$\phi_\gamma = \phi_\pm$, if $\theta_\gamma = \theta_\pm$
Tripe interactions	$\phi_\gamma, \phi_\pm = 0$, if $\theta_\gamma = \theta_\pm$

after the establishment of kinetic equilibrium. Such triple interactions, both direct and inverse, are indeed essential in achieving the thermal equilibrium. The presence of the kinetic equilibrium allowed us to simplify the calculations of triple interactions.

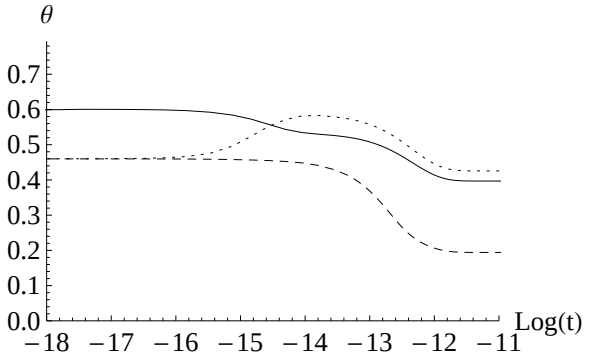

Figure 1. Temperature dependence of time for $\rho = 10^{24}$ erg/cm^3 and $B = 1$. Temperatures of photons, electrons coincide and protons are shown by firm, dotted and dashed curves respectively. Temperatures of electrons and positrons coincide. Time is measured in seconds.

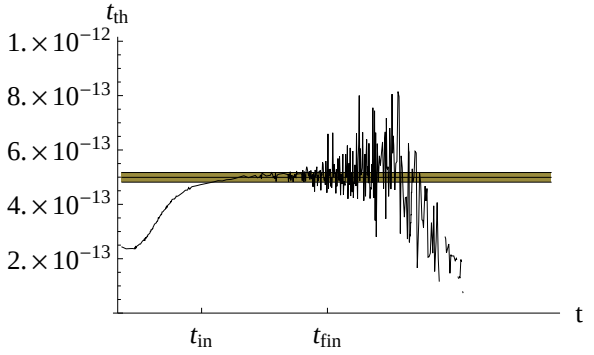

Figure 2. Relaxation time scale (26) for $\rho = 10^{24}$ erg/cm^3 and $B = 1$. It is clear that this quantity saturates to a certain value. The horizontal lines mark this saturation value, as well as one-sigma deviations from it. The time interval of the averaging is confined by $t_{in} = 10^{-12}$ sec and $t_{fin} = 2.5 \cdot 10^{-12}$ sec respectively. Time is measured in seconds.

In presence of protons there are two additional time scales: proton-proton Coulomb scattering $\tau_{pp} \sim (m_p/m_e)^{1/2} (n_\pm/n_p)\, \tau_{ee}$, and proton-electron

Coulomb scattering with $\tau_{ep} \sim \left(m_p c^2/\varepsilon\right)\tau_{ee}$, where τ_{ee} is the Bhabha scattering time scale. The former process may lead to distribution function for protons (9) with $T_p \neq T_\pm$, while the latter makes $T_p = T_\pm$. It is possible to have $t_{ep} < t_{pp}$ in the case of large enough proton concentration. The chemical relaxation (thermalization) time scale is usually computed as

$$\tau_i = \lim_{t\to\infty}\left\{[F_i(t) - F_i(\infty)]\left(\frac{dF_i}{dt}\right)^{-1}\right\}, \qquad (25)$$

where F_i is one of the quantities θ_i, φ_i, n_i, or ρ_i.

We solved the Boltzmann equations with parameters (ρ, B) in the range given by Eqs. (3) and (8). Totally 78 models has been computed, starting from nonequilibrium configuration described above, until the reaching of steady solution. For each model we computed the corresponding time scales for all particles of i kind. For practical purposes instead of (25) we used the following approximation

$$\tau_{th} = \frac{1}{t_{fin} - t_{in}}\int_{t_{in}}^{t_{fin}}[\theta(t) - \theta(t_{\max})]\left(\frac{d\theta}{dt}\right)^{-1} dt, \quad (26)$$

with $t_{in} < t_{fin} < t_{\max}$, $t_{\max}$ is the moment of time where steady solution has been reached, t_{in} and t_{fin} are the boundaries of time interval over which the averaging is performed.

Typical example of temperature dependence on time for one of the models with $\rho = 10^{24}$ erg/cm^3 and $B = 1$ is shown in Fig. 1. Clearly there is no common temperature for all particles, but this numerical effect comes from quite poor energy resolution: we used only 20 grid intervals. While such poor resolution affects particle spectra, it is not relevant for computation of the time scales which depend mainly on the total energy density and number density of protons. In fact we used a special interpolation in order to obtain the exact values of energy and number densities of all particles on our finite grid. Computations with better energy resolution do not show sensitivity of thermalization time scales to the precise form of particle spectra on the grid.

The relaxation timescale of protons (26) is shown in Fig. 2 for the same particular model. It is clear that this quantity saturates to a certain value which marks the approach to thermal equilibrium. The horizontal lines mark this saturation value, as well as one-sigma divinations from it. The time interval of the averaging is confined by $t_{in} = 10^{-12}$ sec and $t_{fin} = 2.5\cdot 10^{-12}$ sec respectively. The noice-like behavior of the relaxation time after t_{fin} is due to numerical effect: while the value of the temperature saturates, its derivative becomes small. As a result, the expression inside the integral in (26) becomes large in absolute value.

In fact there are three thermalization processes: one of electron-positron-photon component, one of proton component, and the final thermalization when all particles reach the same temperature [13]. We are interested here in final thermalization, which is given by

$$t_{th} \simeq Max\left[\tau_{3p}, Min\left(\tau_{ep}, \tau_{pp}\right)\right]. \qquad (27)$$

Our results on thermalization time scales of pair-photons component along with proton one will be presented elsewhere [21]. The values of final thermalization time scales as functions of total energy density for selected B parameter are shown in Fig. 3. The error bars mark the one-sigma deviations in determination of the time scale.

One can inquire how large is the difference between the exact time scales, computed numerically, and the one estimated by order-of-magnitude arguments (27). The comparison is made in Fig. 4. The set of points, fitted by the quadratic spline represent estimated from (27) thermalization time scales. In contrast, computed from (26) values of the thermalization time scale are sometimes two order of magnitude different from the estima-

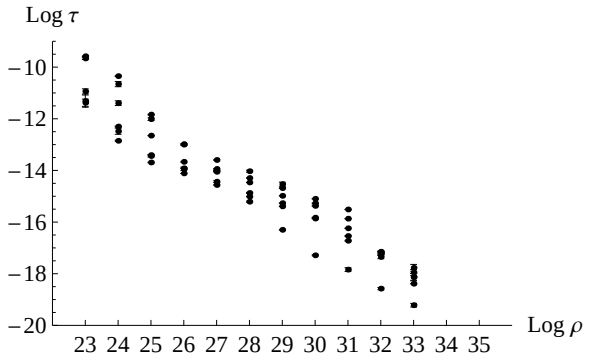

Figure 3. Final thermalization time scale as function of total energy density for selected B parameter. Energy density is measured in erg/cm^3, time is seconds.

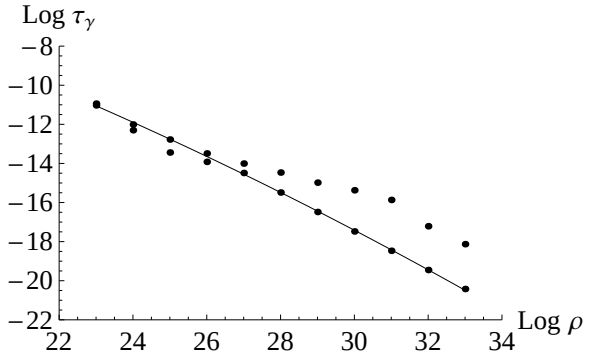

Figure 4. Comparison between the thermalization time scales computed from (26) and estimated from (27) as function of total energy density. Energy density is measured in erg/cm^3, time is seconds. The values, estimated from (27) are joined by the curve.

tion. Moreover, the deviation occurs in both directions and sometimes appears as underestimation, sometimes as overestimation. It is clear therefore that the order-of-magnitude estimation cannot produce satisfactory results.

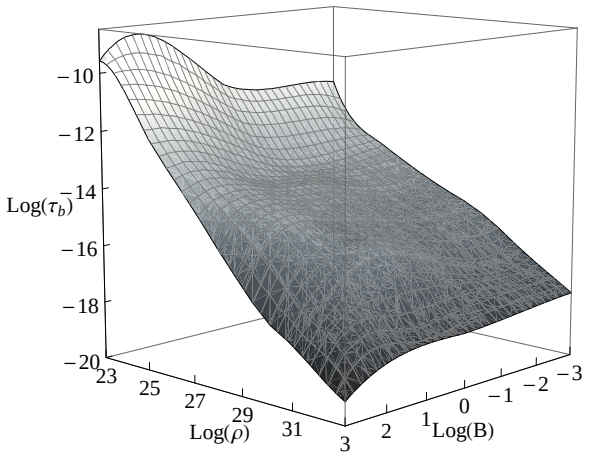

Figure 5. The final thermalization time scale as function of total energy density and baryonic loading parameter. Energy density is measured in erg/cm^3, time is seconds.

The three-dimensional figure showing final thermalization time scale as function of both energy density and baryonic loading is shown in Fig. 5. There we used interpolation between the nodes with computed values of parameters (ρ, B). It is clear that for large baryonic loading the dependence of the thermalization time scale is steeper than for small B. At the same time, while for small energy densities the time scale decreases with decreasing B (due to decrease of the temperature in thermal equilibrium), it remains almost constant for large energy densities (due to the fact that baryons become more energetic and nearly relativistic).

CONCLUSIONS

We developed a code for numerical solution of relativistic Boltzmann equations for optically thick electron-positron plasma with baryonic loading. The collisional integrals include direct and inverse binary interactions such as Compton, Bhabha and Møller scattering, electron-proton and proton-proton scattering, electron-positron pair creation and annihilation into two photons. In addition, direct and inverse triple interactions such as relativistic bremsstrahlung, double Compton scattering, three photon annihilation and radiative pair creation are included.

This code has been used for the computation of thermalization time scale in homogeneous isotropic electron-positron-photon plasma with proton loading. These time scales depend on two parameters, which are chosen as total energy density and baryon loading. We explored the wide range of energy densities and proton loading, corresponding to the temperature range $0.05 \leq k_B T \leq 50$ MeV, and spanning from energy-dominated to matter-dominated plasma, while protons always remain nonrelativistic.

In this parameters range, typical for GRB sources the final thermalization time scale is always $\lesssim 10^{-10}$ sec in the entire parameter range. The main result of this paper, Fig. 5 clearly shows highly nonlinear dependence of thermalization time scale on our parameters. It also becomes clear that order-of-magnitude estimations cannot predict the dependence of thermalization time scales on energy density and on baryonic loading, and are sometimes several orders of magnitude off.

REFERENCES

1. G.S. Bisnovatyi-Kogan, Y.B. Zel'dovich, and R.A. Synaev, Sov. Astron. **15**, 19 (1971).
2. A.P. Lightman, Astroph. J. **253**, 842 (1982).
3. R. Svensson, Astroph. J. **258**, 335 (1982).
4. R. J. Gould, Phys. Fluids **24**, 102 (1981).
5. S. Stepney, Mon. Not. R. Astron. Soc. **202**, 467 (1983).
6. P.W. Guilbert and S. Stepney, Mon. Not. R. Astron. Soc. **212**, 523 (1985).
7. J. Goodman, Astroph. J. **308**, L47 (1986).
8. T. Piran, Phys. Rep. **314**, 575 (1999).
9. R. Ruffini, J. D. Salmonson, J. R. Wilson, and S.-S. Xue, A&A **350**, 334 (1999).
10. R. Ruffini, G.V. Vereshchagin, and S.-S. Xue, Phys. Rep. (2009), in press.
11. H. B. J. Koers and R. A. M. J. Wijers, MNRAS **364**, 934 (2005).
12. A.G. Aksenov, R. Ruffini, and G.V. Vereshchagin, *Phys. Rev. Lett.* **99**, 125003 (2007)
13. A.G. Aksenov, R. Ruffini, and G.V. Vereshchagin, *Phys. Rev. D* **79**, 043008 (2009)
14. S.T. Belyev and G.I. Budker, *Dokl. Akad. Nauk SSSR* **107**, 807 (1956). [Sov. Phys. Dokl. **1**, 218 (1956).]
15. D. Mihalas, *Foundation of Radiation Hydrodynamics* (Oxford, New York, 1984).
16. G Hall and J.M. Watt, *Modern Numerical Methods for Ordinary Differential Equations* (Oxford University Press, Oxford, 1976).
17. L.D. Landau and E.M. Lifshitz, *Physical Kinetics* (Elsevier, 1981).
18. I.P. Ochelkov, O.F. Prilutskii, I.L. Rosental, and V.V. Usov, L.D. *Relativistic kinetics and hydrodynamics* (Moskow, Atomizdat, 1979).
19. E.M. Lifshitz, L.P. Pitaevskii, and V.B. Berestetskii *Quantum Electrodynamics* (Elsevier, New York, 1982).
20. J. Ehlers, Survey of general relativity theory, in *Relativity, Astrophysics and Cosmology*, pages 1–125 (1973).
21. A.G. Aksenov, R. Ruffini, and G.V. Vereshchagin, in preparation.